# 15A.1 RAPID TROPICAL CYCLONE TRANSITIONS TO MAJOR HURRICANE INTENSITY: STRUCTURAL EVOLUTION OF INFRARED IMAGERY

John A. Knaff [1]
*NOAA/NESDIS*
*Center for Satellite Research and Applications*
*Fort Collins, Colorado*

## 1. INTRODUCTION

The anticipation of rapid intensity changes in tropical cyclones (TCs) remains one of the more difficult TC forecasts. The environmental conditions associated with rapid intensification (RI; changes of 25 kt or greater in 24 hours) have been well documented (e.g., Kaplan and DeMaria 2003). However, it is small scale processes such as the organization and intensity of deep convection near the radius of maximum winds and the related formation and organization of the eye/eyewall complex that ultimately determines the timing of rapid intensity changes.

From a forecasting perspective, these rapid intensity changes are potentially most dangerous when rather weak TCs (i.e., tropical storms and weak hurricanes) rapidly become Major Hurricanes with intensities greater than 95 kt. In such a scenario a relatively easy to mitigate and relatively benign tropical cyclone event becomes a potential life threatening disaster if threatening land. These rapid TC transitions to major hurricane intensity are the subject of this study and will be referred to as rapid intensification to Major Hurricane (RITMH) throughout.

To examine these RITMH events, infrared (IR) imagery is used because these data have high temporal (i.e., at least hourly), and spatial (~5km) resolution and are available for operational forecasts globally with little temporal latency (i.e., less than 15 minutes). It is also relatively well known that several characteristics in IR imagery are related to rapid intensification including:

- Anomalously cold IR (< 70$^{o}$C) cloud top temperatures near the TC center
- Symmetric cloud patterns
- Uniformly out flowing cirrus clouds
- A concentration of deep convection near the center
- Ragged or intermittent eye structures become well defined.

In addition to these characteristics, the animation of the IR imagery used in this study show that preceding the RITMH events there is often a distinct maximum in deep convection that moves outward and dissipates which exposes rotating low-level cloud elements. Other propagating characteristics are observed during or just prior to the rapid intensification periods. These include the observation of:

- Rapidly rotating deep convective elements near the likely radius of maximum winds
- The formation of a warm, mostly cloud free mote surrounding the more convective central region
- The deep convection and associated outflow cirrus clouds rotate cyclonically (often back to front) to fill all quadrants and form distinct banded features.

From the subjective examination of the IR imagery, a conceptual model for RITMH can be developed. However, such a model cannot easily be quantified. The remainder of this study seeks to answer three questions.

1) What are the important propagating features in IR imagery of tropical cyclones that experience RITMH?
2) Can a conceptual model for RITMH and RI events in IR imagery be quantified?
3) Can such characteristics be used to improve the ability to forecast of RITMH and RI events?

## 2. DATASETS

This study makes use of three datasets. Infrared (IR) imagery of Atlantic basin tropical cyclones come from an image archive maintained at CIRA/RAMMB and is described in Mueller et al. (2006). The IR data has been remapped to a Mercator projection and has a 4km resolution. For some case used in this study, IR imagery was obtained from the NOAA CLASS system (CLASS, cited 2008) and remapped to a 4-km Mercator projection. Tropical cyclone location and intensity information comes from the National Hurricane Center's best track dataset maintained in the Automated Tropical Cyclone Forecast (ATCF; Sampson and Schrader 2000) database, some of which is based on a prior dataset described in Jarvinen et al (1984). Forecast probabilities of

[1] Corresponding Author: John Knaff, NOAA/NESDIS, CIRA, Colorado State University, Campus Delivery 1375, Fort Collins, CO 80523-1375, John.Knaff@noaa.gov

rapid intensification are provided from the Rapid Intensification Index (RII) described in Kaplan and DeMaria (2006), which were rerun for the period 2002-2007 (Mark DeMaria, personal communication).

## 3. METHODOLOGY

To examine rapid intensification to Major Hurricane (RITMH) cases a selection procedure was constructed. Once cases were selected, special procedures were developed to create a motion relative IR imagery analyses in cylindrical coordinates and with equal temporal frequencies. Using the resulting cylindrical grids complex empirical orthogonal functions (CEOFs) were constructed to determine important propagating features associated with RITMH cases. RITMH case selection is discussed in section 3.1, and the analysis of the imagery is discussed in section 3.2.

To examine whether the CEOFs may be useful in better predicting rapidly intensifying tropical cyclones, the RII index along with the initial intensity is used to find cases during 2002-2007 that rapid intensification was likely. Using these cases, the most important propagating features in the IR imagery are estimated using the loading patterns (i.e., CEOFs) created from the RITMH cases. These features are then examined for their ability to provide information helpful for better anticipating the timing of RI events. The procedures used for selecting rapidly intensifying cases and how CEOF information is utilized are discussed in section 3.3.

### 3.1 RITMH case selection

The selection of the RITMH cases was based on best track intensity data. TCs selected had initial intensities between 45 and 85 kt, obtained a intensity of at least 100 kt within 24 hours, and experienced a 40kt per 24h intensification rate or greater. Only the first case of RITMH was used for each storm. This 24-h period is referred to as the RITMH period. These cases also represent the most extreme RI periods in the best track record. The cases were then matched up with the IR imagery datasets available in both the CIRA IR image archive and on NOAA's CLASS website. Imagery was collected for the period 24 hours prior to and 24 during RITMH. This results in 25 cases shown in Table 1. Average conditions for all cases are also provided in Table 1.

### 3.2 Image analysis procedures

For the purpose of this study it is advantageous to conduct analyses in a cylindrical and in a motion rotated framework. To reformat the existing IR imagery, the best track is first fit to a cubic spline from which a location can be found for each image time. Using the track information the center in the imagery and the concurrent 6-hourly motion are first found for each image. Then a variational data analysis method (or filter) is used to map each 4km IR image to a cylindrical grid with the direction of motion facing north/upward. The resulting cylindrical grid has 101 radial points and 72 azimuthal points with a resolution of 4km x $5^o$. The filter weights produce half-power wavelengths that are 32km and $45^o$ in the radial and azimuthal directions, respectively.

The IR imagery used in this study is typically available in at least half-hourly intervals; however the occasional data gap cause by a corrupt or missing image does occur. Also the satellite eclipse period also occurs around the time of the solar equinox and last about 3 hours. However to conduct CEOF analysis, the input data must have equal time intervals. To both estimate missing image times and to equally space the data for CEOF analyses each grid point is interpolated to equal half-hourly intervals using a cubic spline. The 25 RITMH cases are then concatenated together to form the input dataset for CEOF analysis.

To construct the CEOF analysis the input data is first smooth using a 5-point binomial smoothing function and then tapered with zero values at each endpoint. The quadrature and co-quadrature is then estimated using fast Fourier transforms, resulting in a complex 2-dimensional time series representing the original IR imagery data. From this complex time series a complex correlation matrix is then constructed. The resulting real eigenvalues and complex eigenvectors (i.e., CEOFs) are then calculated. From complex times series and the CEOFs principle components are estimated. The spatial amplitude and phase functions and temporal phase and amplitude functions are calculated from the CEOFs and the complex principle components. From this information a detailed spatial and temporal evolution of these cases can be examined. Details about the CEOF construction procedure can be found in Horel (1984) and DeMaria et al. (1989).

**Table 1**. A list of the rapid transition to Major Hurricane cases and their statistics. Shown are the storm name, year, start date (MMDDHH), end date, latitude, longitude, initial intensity (V-S), ending intensity (V-E), and the 24-h change in intensity (Δ). The averages are also shown.

| NAME | Year | Start | End | Lat | Lon | V-S | V-E | Δ |
|---|---|---|---|---|---|---|---|---|
| EMILY | 1987 | 092118 | 092218 | 16.7 | 69.1 | 50 | 110 | 60 |
| GILBERT | 1988 | 091018 | 091118 | 16.2 | 70.7 | 55 | 100 | 45 |
| JOAN | 1988 | 102018 | 102118 | 11.8 | 81.8 | 70 | 110 | 40 |
| CLAUDETTE | 1991 | 090600 | 090700 | 26.6 | 60.3 | 50 | 105 | 55 |
| ANDREW | 1992 | 082200 | 082300 | 25.6 | 71.1 | 55 | 110 | 55 |
| FELIX | 1995 | 081106 | 081206 | 22.9 | 59 | 70 | 110 | 40 |
| OPAL | 1995 | 100312 | 100412 | 27.3 | 88.5 | 80 | 130 | 50 |
| ROXANNE | 1995 | 101000 | 101100 | 20 | 87 | 60 | 100 | 40 |
| EDOUARD | 1996 | 082400 | 082500 | 15 | 45.8 | 70 | 120 | 50 |
| MITCH | 1998 | 102400 | 102500 | 15.5 | 78.4 | 55 | 100 | 45 |
| BRET | 1999 | 082100 | 082200 | 24.7 | 95.1 | 65 | 120 | 55 |
| ISAAC | 2000 | 092300 | 092400 | 14.9 | 35 | 50 | 105 | 55 |
| KEITH | 2000 | 093000 | 100100 | 17.9 | 86.9 | 45 | 100 | 55 |
| ERIN | 2001 | 090818 | 090918 | 32.4 | 62.8 | 60 | 105 | 45 |
| IRIS | 2001 | 100712 | 100812 | 17.1 | 84 | 75 | 120 | 45 |
| MICHELLE | 2001 | 110206 | 110306 | 18.8 | 84.3 | 60 | 105 | 45 |
| FABIAN | 2003 | 082918 | 083018 | 17.3 | 49.2 | 60 | 100 | 40 |
| ISABEL | 2003 | 090712 | 090812 | 17.1 | 42 | 65 | 110 | 45 |
| IVAN | 2004 | 090418 | 090518 | 10.2 | 46.8 | 55 | 110 | 55 |
| DENNIS | 2005 | 070618 | 070718 | 18.5 | 76.1 | 60 | 100 | 40 |
| EMILY | 2005 | 071318 | 071418 | 12.9 | 64.9 | 55 | 100 | 45 |
| RITA | 2005 | 092006 | 092106 | 24.2 | 84 | 60 | 110 | 50 |
| WILMA | 2005 | 101800 | 101900 | 16.6 | 81.8 | 55 | 130 | 75 |
| GORDON | 2006 | 091300 | 091400 | 27.3 | 57.4 | 65 | 105 | 40 |
| AVERAGE | | | | 19.5 | 69.3 | 60 | 109 | 49 |

3.3 Assessing RI predictive capabilities

To assess the capabilities of CEOF information to improve the prediction of TC rapid intensification events, only cases in which rapid intensification is likely based on environmental and cloud-top temperature conditions are examined. The likelihood of rapid intensification, defined as a 25kt per day increase in intensity, is estimated using the Kaplan and DeMaria RII (based upon discriminant analysis and screening methodologies). The RII is given as a probability. In operational testing the RII had ~ 10% probability of detection and ~55% false alarm ratio (John Kaplan, personal communication) for all cases. In this study, however the cases are additionally screened by initial intensity (i.e., 45kt < intensity < 85kt) and by a threshold/mean value of RII (i.e., ≥20% RII ≥20%, for either the discriminant or scaled versions of RII). Additionally, if the intensification potential was less than 25 kt the case was not used. The final cases also had to have two or more consecutive periods where these conditions were met. The remaining cases represent roughly the top 40% of RII values 2002-2007 and resulted in 31 different TCs (Table 2). Twenty-one of these storms had at least one period of RI (i.e. 25kt/d) and 14 storms had at least one period of RITMH (eight TCs were also in the developmental dataset). However, there were 149 six-hourly times. Nonetheless, the RII works well as 48% and 27% of these cases being were associated with RI and RITMH, respectively. These findings suggest that the RII index does a good job of indicating which storms will intensify rapidly, but the exact timing of when the RI and RITMH begins remains relatively difficult to predict.

**Table 2:** Cases that the rapid intensification index (RII) has a value of 20% or greater, had initial intensity of 50 to 85 kt, were not affected by landfall (i.e., within 50 nmi) during the 2002-2007 period. Also shown is whether the case experienced a period of rapid intensification (i.e., 25kt in 24 h) or a period of RITMH as defined in section 3.1.

| Year | Storm | RI | RITMH |
|---|---|---|---|
| 2002 | Dolly | NO | NO |
| 2002 | Isidore | YES | NO |
| 2002 | Lili | YES | YES |
| 2003 | Claudette | NO | NO |
| 2003 | Fabian | YES | YES |
| 2003 | Isabel | YES | YES |
| 2003 | Larry | NO | NO |
| 2003 | Nicholas | NO | NO |
| 2003 | Odette | NO | NO |
| 2004 | Charlie | YES | NO |
| 2004 | Danielle | YES | NO |
| 2004 | Frances | YES | YES |
| 2004 | Ivan | YES | YES |
| 2004 | Jeanne | YES | NO |
| 2004 | Karl | YES | YES |
| 2005 | Dennis | YES | YES |
| 2005 | Emily | YES | YES |
| 2005 | Katrina | YES | NO |
| 2005 | Maria | YES | NO |
| 2005 | Nate | NO | NO |
| 2005 | Ophelia | NO | NO |
| 2005 | Philippe | NO | NO |
| 2005 | Rita | YES | YES |
| 2005 | Wilma | YES | YES |
| 2005 | Beta | YES | YES |
| 2006 | Florence | YES | NO |
| 2006 | Gordon | YES | YES |
| 2006 | Helene | YES | YES |
| 2007 | Dean | YES | YES |
| 2007 | Felix | YES | YES |
| 2007 | Noel | NO | NO |

It is a reasonable assumption that structural differences that can be found in patterns in the IR imagery or other remotely sensed imagery (e.g., Kieper (2008)) may help better predict the onset of RI and RITMH events. Using the CEOFs (i.e., loadings) and the imagery record from the storms in Table 2, the real-time complex principle components and thus phase and amplitude information is then estimated. The time series of real and imaginary parts of the principle components are then examined for their ability to indicate structures that are conducive for RI and RITMH events. Using these properties, a probability associated with having an IR structure that is conducive for RI is created. Results of this analysis are shown in section 4.2.

## 4. RESULTS

### 4.1 Complex EOFs associated with RITMH

Using the IR imagery from the RITMH cases listed in Table 1, complex principle component analysis was performed. The spatial amplitude and phase functions are shown in Fig.1. The first CEOF appears associated with the variation of mean standardized IR temperatures in the RITMH cases and explains 29.8% of the variance. The second through sixth CEOF are clearly related to propagating features and explain 13.8, 10.4, 7.8, 4.6 and 3.9% of the normalized variance, respectively. The second (fourth) CEOF appears primarily related to cyclonically (anti-cyclonically) rotating features beyond 150km radius. The third CEOF is related to the symmetric pulsing of IR brightness temperatures near the TC center, which seem to be sometimes tied to diurnal period. The fifth CEOF is most curious as it appears related to rotating IR features near the radius of maximum winds and the formation of a cloud free mote region near 150km. The sixth and final CEOF shown appears related to variations of the warm eye features in the imagery.

To show the evolution of these patterns Fig.2 shows the composite averages of phase and amplitude functions from the 25 RITMH cases. In this figure, the real component is orientated along the x-axis and the imaginary component is orientated along the y-axis. The amplitude is indicated by the length of the arrow. From these results, it appears that some of the structural evolution of the IR imagery coincides or precedes the beginning of RITMH, which is located at the midpoint on the x-axis with a value of zero hours.

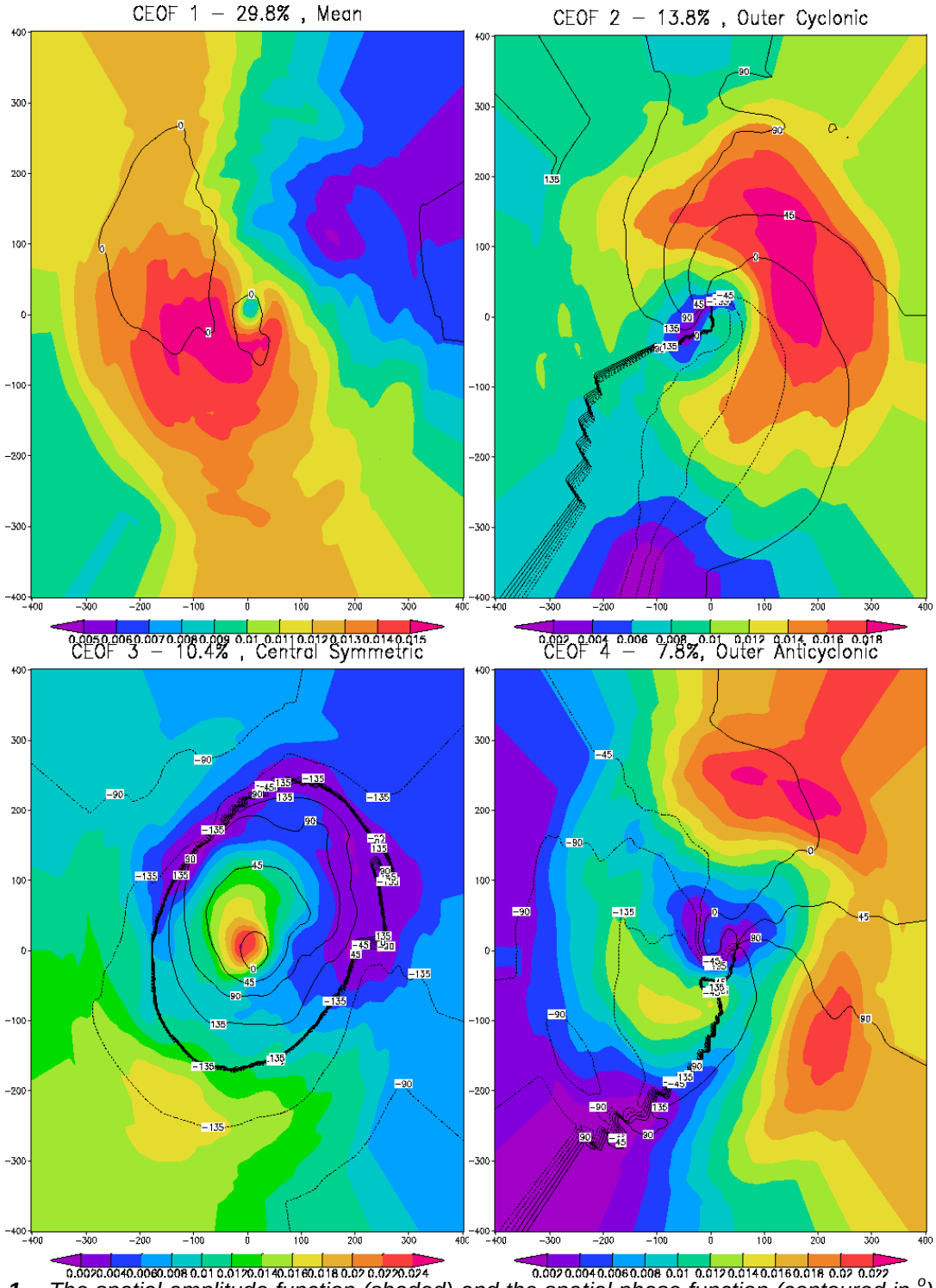


***Figure 1.*** *The spatial amplitude function (shaded) and the spatial phase function (contoured in $^{o}$) for the first six complex CEOFs for the 25 cases of RITMH shown in Table 1.*

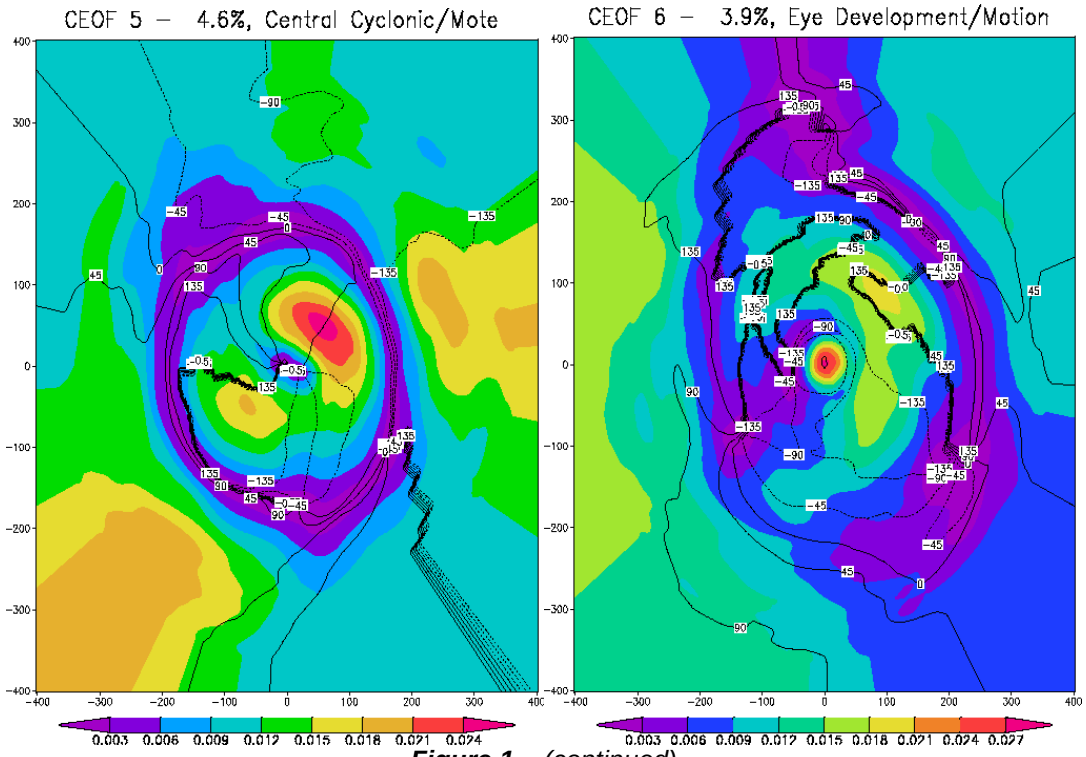


***Figure 1.*** *(continued)*

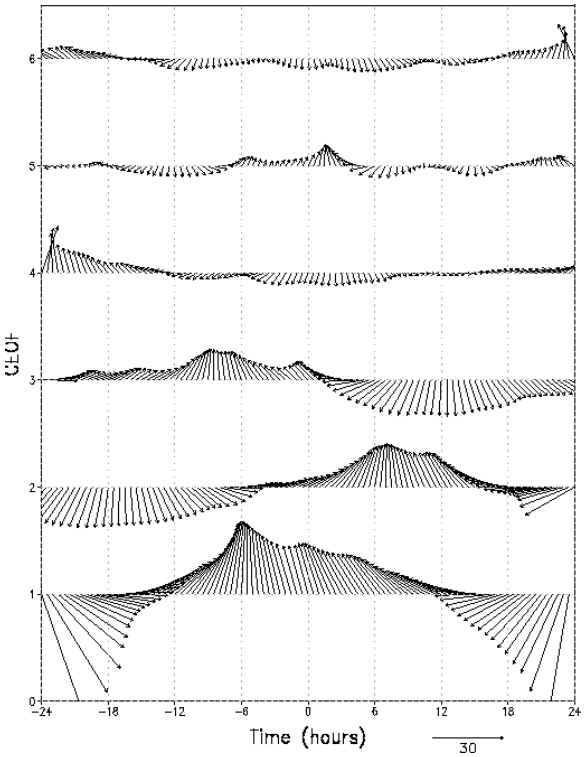


***Figure 2.*** *The composite average of the temporal amplitude, given by the vector length, and the phase indicated by the direction of the first six complex principle components associated with the 25 cases of RITMH shown in Table 1.*

4.2 Using IR Structure to Predict RI

By repeating the spatial and temporal interpolation steps to the IR imagery for the cases in Table 2, a 2-dimentional (r x θ) complex time series can be created for each case. Then using the CEOFs from the analyses shown in Fig. 1-2, real eigenmodes and complex principle components (CPCs) can be created for each time period. Instead of using the amplitude and the phase functions, the real and imaginary parts of the CPCs are examined via compositing and visual inspection for potential to better predict RI and RITMH events associated with the cases shown in Table 2.

The examination of the CPCs from these cases shows that the CEOF analysis is capturing some IR structures that appear consistently related to intensity changes. In particular the imaginary parts of the of CPC-1 and CPC-2 and the real parts of CPC-2 and CPC-3 can be combined to estimate intensity change and a probability of RI based on the 149 6-hourly cases in Table 2. Physically these factors can be physically interpreted as:

- AIMAG(CPC-1): positive values are generally related to cooling of the broad mean.

- CPC-2 : when both real and imaginary components are positive, this indicates that the cyclonically rotating features are orientated right front (positive-less convection) to left rear (negative-more convection)
- REAL(CPC-3): When negative, the maximum of pulsing symmetric convection (i.e., cooler IR temperatures) is located near the center and the minimum (i.e., warmer IR temperatures) is located between 50 and 150 km this pulse is typically moving outward – indicating recent or current active deep convection near the center.

Figure 3 shows the individual eigenmodes 1-3 and the superposition of these three modes for Hurricane Dean (2007) on Aug. 15 1745 UTC when the factors AIMAG(CPC-1), REAL(CPC-2), AIMAG(CPC-2) and REAL(CPC-3) were 87,57,79, and10, respectively (i.e., the correct configuration for RI and RITMH).

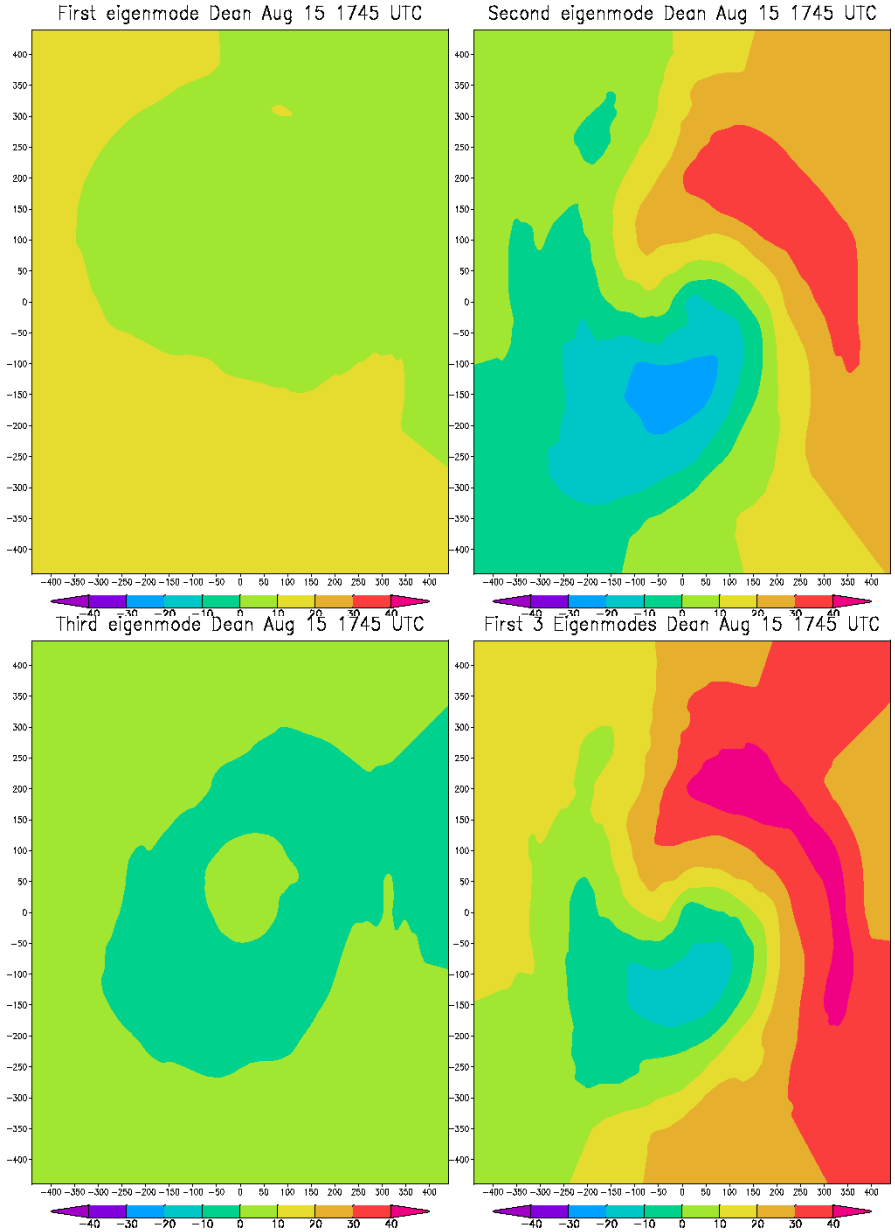


***Figure 3.*** *The first three eigenmodes calculated for Hurricane Dean on 15 Aug 2007 at 1745 UTC. Shown are the contours of brightness temperature anomalies ($^{o}$K) for eigenmode 1, 2, 3 and the combination of these three eigenmodes (bottom Left). Storm motion is upward in all panels.*

An estimate of the probability of RI can be developed by combining these four predictors in a multiple regression scheme. The estimated probabilities are similar in magnitude to those of the RII index, and appear independent to the RII probabilities (i.e., their cross correlation is zero). Figure 4 shows the average of the two versions of Kaplan and DeMaria RII (calculated by adding the two probability estimates and dividing by two), and the RI probability predicted using only the CPCs. The results of the two methods produce similar statistical results, but have quite different scatter diagrams (Fig. 4). Since the two methods are independent, the addition of these two probabilities produces a new probability index shown in Figure 5 versus intensity change. Reliability diagrams (not shown) indicate that both the averaged Kaplan & DeMaria RII (ARII) method and CPC-based method are low biased. In addition the ARII is also under confident. Adding the ARII and CPC-based probabilities together results in a non-biased probability estimate that is only slightly under confident and much better calibrated.

Table 3 shows the results from contingency table analysis for the ARII and addition of the ARII and the CPC-based probabilities (ARII+CPC) based on various probability thresholds. It is remarkable how well the ARII probabilities predict RI and RITMH when the results are screened by initial intensity, by potential intensity and by a probability threshold (i.e., at least 20% for either of the RI indices). Findings show that 86% of the RI cases are correctly identified, with a false alarm ratio of 43%. These results can be improved by incorporating information available from IR imagery. By using the CPC-based probabilities along with the ARII probabilities, the ability to discriminate yes from no is improved as shown by the statistics shown in Table 3. This is also true for the prediction of RITMH events, also in Table 3. These improvements are realized from better prediction of the timing of RI and RITMH events when the environmental conditions are favorable (i.e., as measured by the ARII).

## 5. SUMMARY AND CONCLUSIONS

This pilot study examines whether propagating (and stationary CEOF-1) features in routine IR imagery can be used to predict RI and RITMH events more accurately. This study concentrated on TCs that intensified from a weak hurricane or strong tropical storm to Major Hurricane in less than 24 hours. Specifically, the following questions were addressed and answers provided:

1) *What are the important propagating features in IR imagery of tropical cyclones that experience RITMH?*
   **ANS**: Figure 1 and 2 show the most important propagating normalized variance features in the IR imagery of RITMH events.
2) *Can a conceptual model for these RITMH events in IR imagery be quantified?*
   **ANS:** Yes, Fig. 4 shows how such information can be combined to form a probabilistic forecast using the predictors described in section 4.1
3) *Can such characteristics be used to improve the ability to forecast of RITMH and RI events?*
   **ANS:** Preliminary results suggest that the structural characteristics diagnosed from the patterns in Fig. 1 can be utilized in an automated manner to better predict the timing of RI and RITMH events given favorable environmental conditions indicated by the Kaplan RII.

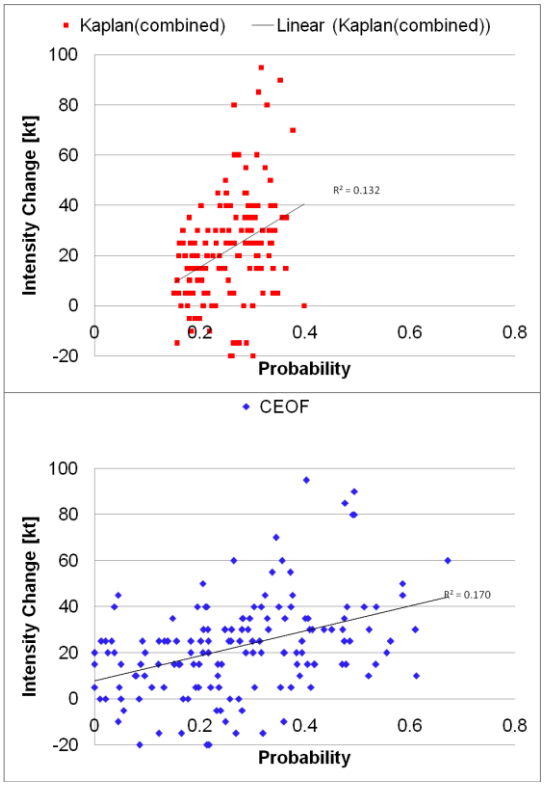


***Figure 4.*** *Scatter plots of the probabilities associated with the averaged Kaplan & DeMaria RII and the CPC-based method versus the future 24-h intensity change.*

In this study, the Rapid Intensification Indices (discriminant and scaled versions) were evaluated for those cases with initial intensity of 50 to 80 kt, a RII (either method) of at least 20%, and potential intensity greater than 25 kt. The results suggest that the combined RII or ARII does a good job at discriminating RI and RITMH events when stratified in this manner with 86% probability of detection and a 43% false alarm ratio.

These results are preliminary, but suggest that information available in IR imagery can be utilized to better predict the timing of RI and RITMH events. The simple regression based probabilities can be improved upon by using more suitable methods for making probabilistic forecasts. Furthermore, it seems that such a method could be completely automated and routinely prepared for the forecast cycle. Future work will also involve the examination of more TC cases (and in multiple TC basins) and the development of an automated strategy to provide such information either directly into the RII methodology or separately for use in real-time intensity change forecasting.

Table 3. Contengency table-based verification results for the average of the Kaplan RI indices (ARII) and the sum of the ARII and the CPC-based probability of RI as a function of a probability threshold. Shown are the accuracy, bias, probabilty of detection (POD), probability of false detection (POFD), the false alarm ratio (FAR) and the critical success ratio(CSR). Verification is shown for both Rapid Intensification and Rapid Intensification to Major Hurricane (both described in the text).

| **Prediction of Rapid Intensification** | | | | | | | |
|---|---|---|---|---|---|---|---|
| **Method** | **Threshold p** | **Accuracy** | **Bias** | **POD** | **POFD** | **FAR** | **CSR** |
| ARII | 0.20 | 0.39 | 1.52 | 0.86 | 0.62 | 0.43 | 0.52 |
| ARII | 0.30 | 0.60 | 0.60 | 0.39 | 0.19 | 0.35 | 0.32 |
| ARII | 0.40 | 0.52 | 0.00 | 0.00 | 0.00 | N/A | 0.00 |
| ARII+CPC | 0.20 | 0.50 | 1.06 | 1.0 | 0.96 | 0.51 | 0.49 |
| ARII+CPC | 0.30 | 0.59 | 1.69 | 0.93 | 0.71 | 0.45 | 0.53 |
| ARII+CPC | 0.40 | 0.68 | 1.32 | 0.83 | 0.45 | 0.36 | 0.56 |
| ARII+CPC | 0.50 | 0.66 | 0.40 | 0.57 | 0.25 | 0.51 | 0.45 |
| **Prediction of Rapid Intensification to Major Hurricane** | | | | | | | |
| **Method** | **Threshold p** | **Accuracy** | **Bias** | **POD** | **POFD** | **FAR** | **CSR** |
| ARII | 0.20 | 0.52 | 2.75 | 0.97 | 0.65 | 0.64 | 0.35 |
| ARII+CPC | 0.20 | 0.28 | 3.65 | 1.0 | 0.97 | 0.73 | 0.27 |
| ARII+CPC | 0.30 | 0.35 | 3.05 | 0.97 | 0.76 | 0.68 | 0.31 |
| ARII+CPC | 0.40 | 0.62 | 2.38 | 0.97 | 0.51 | 0.58 | 0.40 |
| ARII+CPC | 0.50 | 0.73 | 1.50 | 0.75 | 0.27 | 0.50 | 0.42 |

**ACKNOWLEDGMENTS:**

This work is supported by NOAA Grant NA17RJ1228. The views, opinions, and findings in this report are those of the authors and should not be construed as an official NOAA and or U.S. Government position, policy, or decision.

**REFERENCES:**

CLASS, cited 2008: NOAA's Comprehensive Large-Array Stewardship System, available at http://www.class.ngdc.noaa.gov/saa/products/welcome.

DeMaria, M., J. M. Davis, and D. M. Wojtak 1989: Observations of mesoscal wave disturbances during the genesis of atlantic lows experiment. *Mon. Wea. Rev.*, **117**:4, 826-842.

Jarvinen, B. R., C. J. Neumann, and M. A. S. Davis, 1984: A tropical cyclone data tape for the North Atlantic basin, 1886-1983: Contents, limitations and uses. NOAA Tech Memo. NWS NHC 22, Coral Gables, FL, 21pp. . [Available from NTIS, Technology Administration, U.S. Dept. of Commerce, Springfield, VA 22161]

Horel, J. D., 1984: Complex principle component analysis: Theories and examples. *J. Climate and App. Meteor.*, **23**, 1660-1673.

Kaplan, J., and M. DeMaria, 2006: Estimating the likelihood of rapid

intensification in the Atlantic and E. Pacific basins using SHIPS model data. *AMS 27th Conference on Hurricanes and Tropical Meteorology.* 24-28 April, Monterey, CA.

_____, and _____, 2003: Large-scale characteristics of rapidly intensifying tropical cyclones in the North Atlantic basin, *Wea. Forecasting*, **18**:6,1093-1108.

Kieper, M. E., 2008: A technique for anticipating initial rapid increases in intensity in tropical cyclones, using 37 gHz microwave imagery. *28th Conference on Hurricanes and Tropical Meteorology*, 28 April – 2 May 2008, Orlando, Florida.

Sampson, C. R. and A. J. Schrader, 2000: The automated tropical cyclone forecasting system (Version 3.2). *Bull. Amer. Met. Soc*., **81**, 1231-1240.